Technical Report
RAL-TR-2001-012

The Development of Vacuum Phototriodes for the CMS Electromagnetic Calorimeter

K W Bell R M Brown D J A Cockerill P S Flower P R Hobson D C Imrie B W Kennedy
A L Lintern C A X Pattison M Sproston and J H Williams

26th February 2001

COUNCIL FOR THE CENTRAL LABORATORY OF THE RESEARCH COUNCILS

Enquiries about copyright, reproduction and requests for additional copies of this report should be addressed to:

The Central Laboratory of the Research Councils
Library and Information Services
Rutherford Appleton Laboratory
Chilton
Didcot
Oxfordshire
OX11 0QX
Tel: 01235 445384 Fax: 01235 446403
E-mail library@rl.ac.uk

We acknowledge the copyright of Elsevier Publications B.V.. We thank Elsevier Publications B.V. for giving us permission to publish this article.

ISSN 1358-6254

RAL-TR-2001-012

The Development of Vacuum Phototriodes for the CMS Electromagnetic Calorimeter

K W Bell[1], R M Brown[1], D J A Cockerill[1], P S Flower[1], P R Hobson[2], D C Imrie[2], B W Kennedy[1], A L Lintern[1], C A X Pattison[1], M Sproston[1], J H Williams[1]

[1]*Particle Physics Department, CLRC Rutherford Appleton Laboratory, Chilton, UK*

[2]*Department of Electronic and Computer Engineering, Brunel University, Uxbridge, UK*

Abstract

A new generation of vacuum phototriodes (VPTs) has been developed for application in the end cap sub-system of the crystal electromagnetic calorimeter (ECAL) for the CMS experiment at the CERN Large Hadron Collider (LHC). These VPTs must operate with high reliability for at least ten years in an extremely hostile environment. Results are presented from an extensive programme of tests, demonstrating that the required properties of significant gain in a 4 T magnetic field, resistance to ionising radiation, and stable operation with large photocurrents can all be satisfied in a robust, compact, inexpensive device.

(Accepted for publication in Nuclear Instruments and Methods in Physics Research, Section A)

1 Introduction

CMS (Compact Muon Solenoid detector)[1] is one of two general purpose experiments under preparation for the LHC (Large Hadron Collider) at CERN. It is shown schematically in figure 1. It is divided into a 'barrel' section, with various detectors arranged in concentric cylinders around the collision region, and two 'end cap' sections which complete the solid angle coverage. CMS has an overall length of 21.6 m, a radius of 7.5 m, and a total mass of approximately 12500 t. At the heart of the apparatus is a powerful solenoidal magnet with a superconducting coil which is 13 m in length, has a free inner diameter of 5.9 m, and provides a uniform field of 4 T.

Many of the physics processes to be studied at the LHC require the measurement of high energy electrons and photons. Strong emphasis has therefore been placed on incorporating a high resolution electromagnetic calorimeter (ECAL) in the design of CMS[2] (figure 2). In order to minimise the amount of inert material in front of the ECAL, and thus optimise the energy resolution, it is located within the magnetic field volume.

The radiation levels within CMS are generally very much higher than those in current or previous high energy physics experiments. Figures 3a and 3b show the distribution of radiation dose and neutron fluence expected in the region of the electromagnetic calorimeter, after 10 years of operation. The radiation levels increase strongly towards the forward region, at small distances from the beam axis. Designing detectors, which will survive this harsh radiation environment for the lifetime of the experiment, poses a substantial challenge.

The technology chosen for the ECAL uses large monocrystals of lead tungstate[2] (a dense inorganic scintillator) coupled to sensitive photodetectors. The lead tungstate crystals are approximately square in cross section and have a slight taper along their length. They are arranged to point close to, but not precisely at, the collision region. (The 'off-pointing' is to reduce the degradation in performance caused by the inevitable gaps between the crystals.) In the barrel region, which covers the range of pseudorapidity $|\eta| < 1.48$ (25.6° to 154.4° with respect to the beam axis), there are approximately 61000 crystals, with typical dimensions 22x22x230 mm^3. In the end cap regions, which cover the range $1.48 < |\eta| < 3.0$ (25.6° to 5.7° and 154.4° to 174.3° with respect to the beam axis), there are approximately 16000 crystals, with typical dimensions 30x30x220 mm^3.

The properties of lead tungstate are well matched to the needs of the CMS ECAL. It is radiation hard, it has a short radiation length ($X_0 = 0.89$ mm) and the scintillation process is fast, with 80% of the light emitted within 20 ns. The peak of the emission spectrum is conveniently located at 425 nm (Figure 4); however, the light yield measured at the back of the crystals is rather low, of order 60 photons per MeV of deposited energy.

At the LHC, beam crossings occur every 25 ns and the ECAL readout has therefore been designed to operate with a sampling frequency of 40 MHz. In order to achieve the design energy resolution, the energy equivalence of the readout noise is required to be less than 30 MeV/channel for the barrel system and 150 MeV/channel for the end caps, where the particle energies are higher. Because of the low light yield of the crystal, this electronic performance can only be achieved by using photodetectors with internal gain. Furthermore, the photodetectors must operate in a 4 T field and survive the high radiation levels for at least ten years. No devices were previously available which would satisfy the needs of CMS at an affordable price and a substantial programme of development has therefore been required.

The photodetectors which have been developed for the barrel section of the calorimeter are avalanche photodiodes. These are used in pairs to give a total sensitive area of 50 mm^2 and are operated with an avalanche gain of 50. They are described in detail elsewhere[3]. However, silicon devices cannot be used in the end caps since, as can be seen in figures 3a and 3b, the radiation doses and neutron

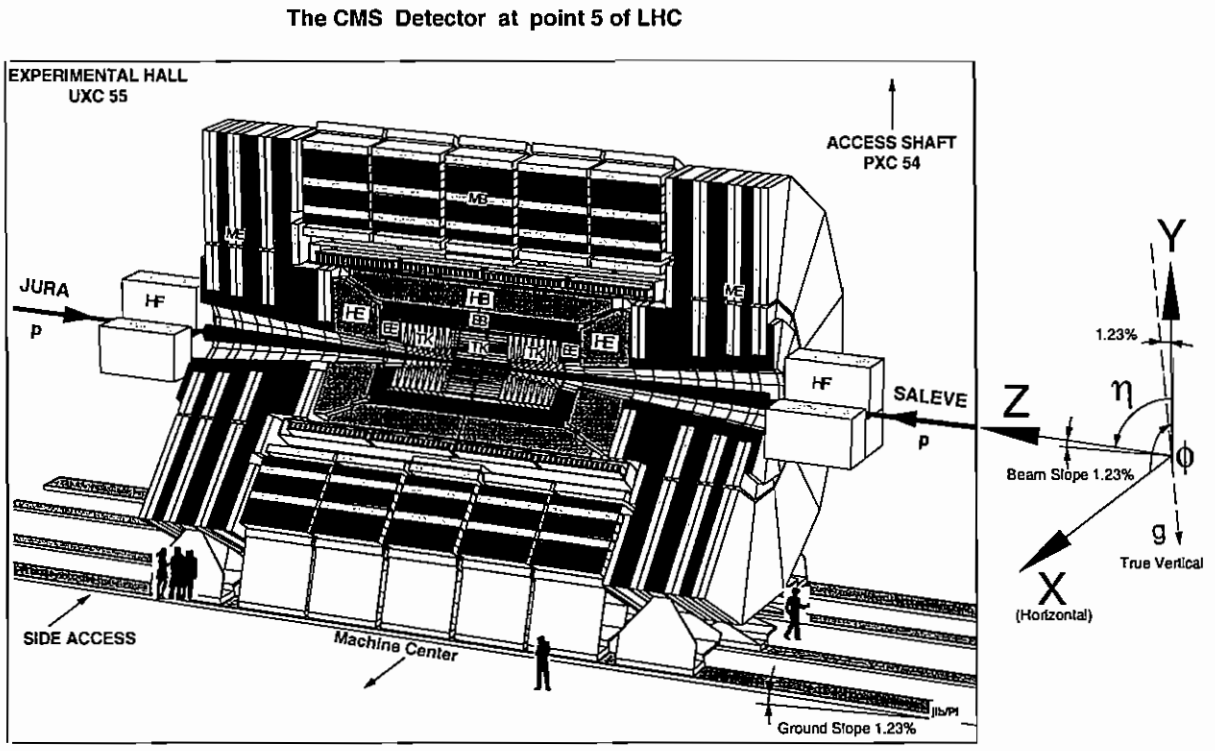

Figure 1: A cut away view of the CMS detector. The end cap section of the electromagnetic calorimeter is denoted by EE, and the barrel section by EB. HE and HB are the corresponding sections of the hadron calorimeter. The superconducting coil of the 4 T solenoid is the structure immediately surrounding HB.

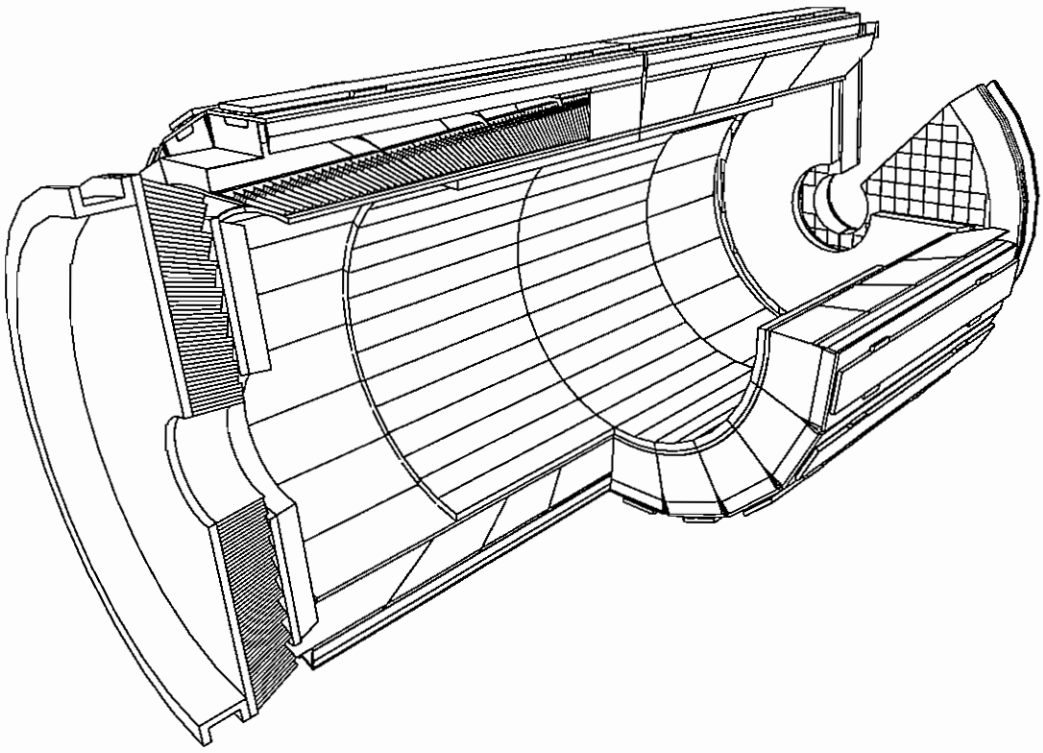

Figure 2: A cut away view of the CMS electromagnetic calorimeter showing the orientation of the crystals in the end cap and barrel sections.

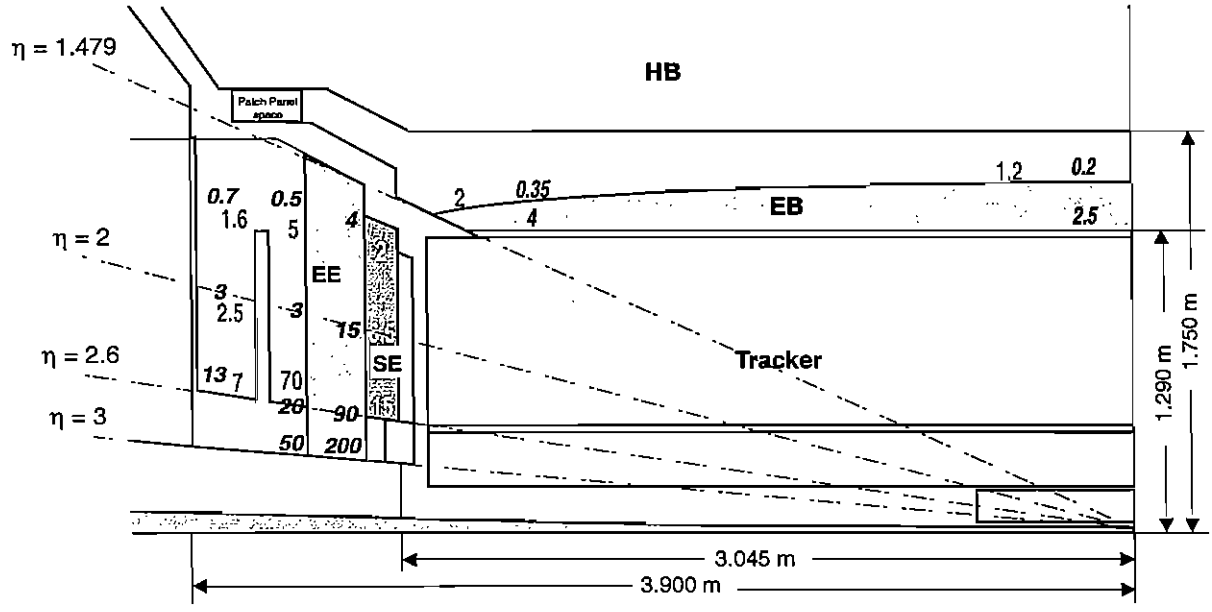

Figure 3a: The estimated radiation dose and neutron fluence in the region of the CMS electromagnetic calorimeter, after ten years of LHC operation. (EE and EB denote the end cap and barrel sections respectively of the electromagnetic calorimeter; HB is the barrel section of the hadron calorimeter.) The numbers in bold italics are doses in kGy, the other numbers are neutron fluences in units of 10^{13} cm^{-2}. The VPTs are located in the region immediately behind the shaded area labelled EE, where the doses range from 0.5 kGy to 50 kGy.

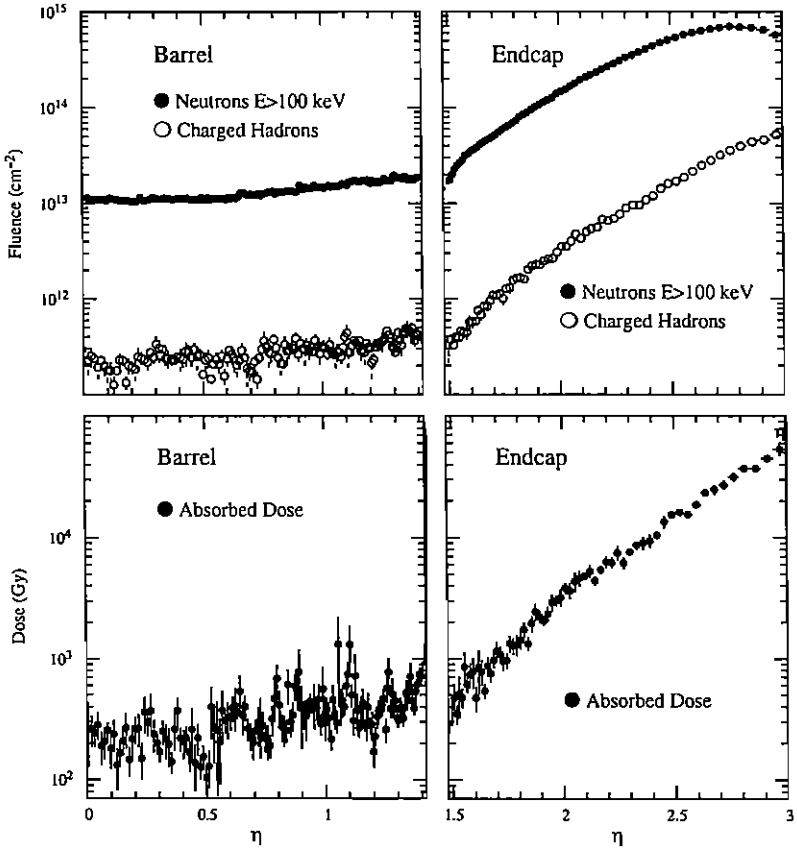

Figure 3b: The neutron (E>100 keV) and charged hadron fluence and absorbed dose immediately behind the ECAL crystals, as a function of pseudorapidity, for 10 years of LHC operation.

fluences are even higher there than in the barrel section and would result in high leakage currents, giving an unacceptably high contribution to the noise[4]. Vacuum phototriodes (VPTs), which are essentially single stage photomultiplier tubes, have therefore been chosen for the end caps. Such devices are potentially very radiation hard and they can be designed to have useful internal gain in a high magnetic field, as long as the angle between the field and the tube axis is not too large. (This latter constraint prevents their consideration for the barrel.)

Here we report studies that have led to the successful development of VPTs for CMS. In the course of this work, prototype devices have been obtained from a number of manufacturers. Here we concentrate on the properties of tubes supplied by Electron Tubes Ltd[5], Hamamatsu Photonics[6] and Photonis[7]. Results from devices produced by Research Institute Electron[8] and Meltz[9] are presented elsewhere[10]. In the remainder of this paper, section 2 addresses the principles of operation, section 3 describes the behaviour as a function of applied voltage and magnetic field. The results of accelerated ageing tests are given in section 4, and irradiation studies are described in section 5. Finally, section 6 shows the performance achieved in a high energy electron beam, with a calorimeter test module instrumented with VPTs.

2 Principles of Operation

Detecting weak photon signals in a strong magnetic field, over a large area, at an affordable price is a long standing challenge in electromagnetic calorimetry, to which vacuum phototriodes offer a practical solution. VPTs were first developed for the end cap lead glass calorimeter for the OPAL experiment at LEP[11]. They have also been used on DELPHI at LEP, both for the end-cap lead glass calorimeter and the 'STIC' detector[12]. The devices developed for OPAL were required to operate in a field of 0.4 T in a low radiation environment, and have operated very successfully for more than ten years. However, the requirements for CMS are much more demanding, most notably because the magnetic field is ten times stronger and the radiation levels are very high. Substantial development has therefore been necessary to apply VPT technology to CMS.

Figure 5a is a photograph of a typical VPT with dimensions appropriate to the CMS application and 5b illustrates schematically the construction. A planar semitransparent photocathode is deposited on the inner surface of a glass faceplate. There is a single dynode in the form of a reflective layer deposited on a planar electrode. The anode takes the form of a metallic mesh located between the photocathode and the dynode, close to the dynode. The tubes developed for CMS have a bialkali photocathode (SbKCs), since the spectral sensitivity is well matched to the emission spectrum of lead tungstate. The same material also forms the active coating of the dynode.

In operation, the photocathode is grounded, the dynode is operated at around $V_D = 600$ V to ensure a high electron secondary emission factor, and the anode voltage is set approximately 200 V higher ($V_A = 800$ V) to optimise the collection of secondary electrons emitted by the dynode. Optical photons incident on the photocathode eject photoelectrons, which are then accelerated towards the anode. A fraction ε of the electrons pass through the apertures in the anode mesh and strike the dynode with a kinetic energy corresponding to the dynode voltage, the remainder are collected by the anode. Of order 20 secondary electrons are ejected by each photoelectron striking the dynode. They are attracted to the anode where a fraction $(1-\varepsilon)$ is collected and the remainder transmitted. The electric field brings the transmitted electrons to rest and accelerates them back towards the anode where a further fraction $(1-\varepsilon)$ is collected. The remaining secondary electrons strike the dynode producing tertiary electrons, some of which are collected on the anode. The production of quaternary electrons by tertiary electrons returning to the dynode is assumed to be negligible.

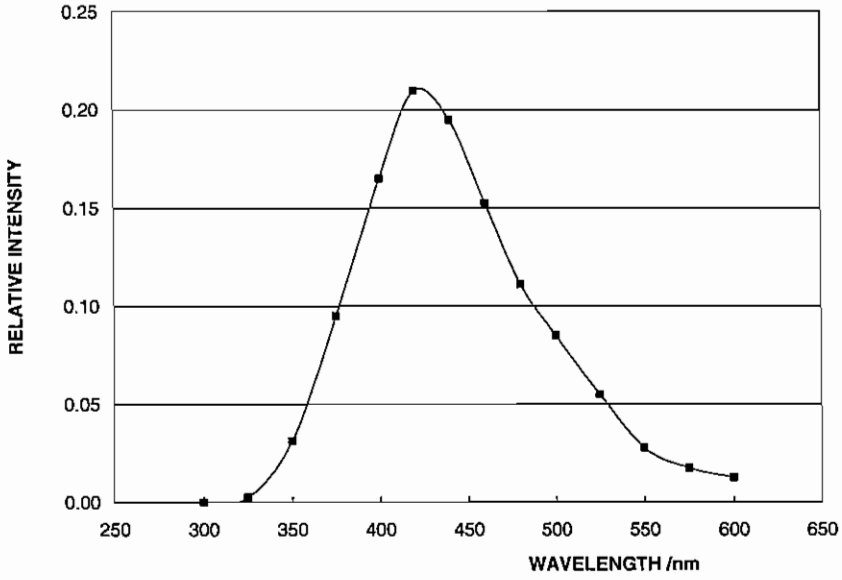

Figure 4: The scintillation emission spectrum for lead tungstate doped with lanthanum[2].

Figure 5a: A prototype one inch diameter vacuum phototriode.

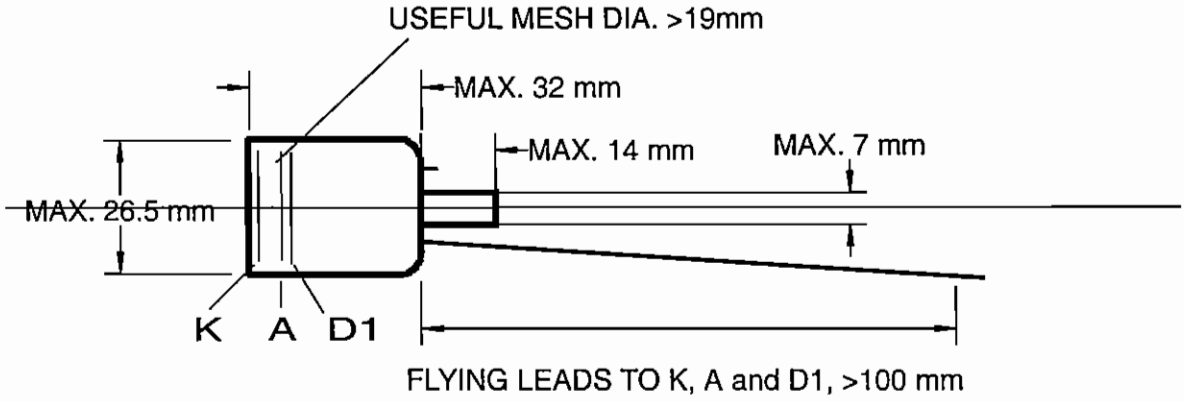

Figure 5b: A schematic view of a vacuum phototriode with the dimensions required for the CMS ECAL. K is the photocathode, consisting of a semitransparent coating on the inner surface of the front window. A is the anode, consisting of a very fine metallic mesh, and D1 is the solid metal dynode, coated with the same material as the photocathode.

Thus the effective gain of the VPT, G, is given approximately by the expression:

$$G = (1-\varepsilon) + m\,\varepsilon\,(1+\varepsilon^2\alpha)\,(1-\varepsilon^2) \qquad 1$$

where $m \sim 20$ is the secondary emission factor and $\alpha \sim 0.5$ is the tertiary emission factor.

In practice, the anode mesh must be supported by a ring of material at its outer circumference, with the result that its effective diameter is significantly less than that of the photocathode. The grid transmission factor for photoelectrons is therefore generally less than that for secondary and tertiary electrons. Equation 1 would indicate that the gain should have a maximum value of 9.5 for values of $m = 20$, $\varepsilon = 0.62$. The gain is insensitive to the precise value of ε, decreasing by less than 2% for values of ε deviating by $\pm$ 10% from the optimum. However, for a VPT with an external diameter of 25 mm, the diameter of the mesh is typically 10% less than overall diameter of the anode, with the result that the gain of the VPT is of order 20% less than this simple prediction. A more complete discussion of these effects may be found elsewhere[13,14].

Equation 1 assumes that the grid transmission probabilities of the initial photoelectrons and the secondary electrons they produce are uncorrelated. In practice, the anode mesh casts a shadow on the dynode and secondary electrons are only emitted in regions illuminated by incident photoelectrons. Nevertheless, in the absence of a magnetic field, the distribution in angle of the emitted electrons, relative to the VPT axis, is sufficient to wash out the grid-like modulation of their spatial distribution by the time they reach the anode plane. Thus equation 1 is valid.

However, in the presence of a strong magnetic field, the drifting electrons are constrained to move in tight helices about the magnetic field lines. At fields of a few Tesla, the cyclotron radii are of the order of a few microns. Since typical anode meshes have pitches of order 10-20 μm, there is an enhanced probability that secondary electrons will pass through the same aperture of the anode grid as the incident photoelectron, and the gain is reduced compared to the expectation of equation 1.

The principal technological challenge in developing a VPT which will provide a useful gain in a strong, quasi-axial magnetic field is therefore to fabricate a large area, thin, self-supporting, conducting grid with a mesh size below ~15 μm and a transparency exceeding 0.5.

In the general case where the magnetic field is not parallel to the tube axis, photoelectrons may be guided on to the wall of the glass envelope before reaching the electrodes, causing a further decrease in response. An additional effect arises since the spiralling electrons are no longer normally incident on the anode plane and the thickness of the mesh becomes important as well as its aspect ratio. This tends to increase the gain at angles up to 40°.

For light pulses of a given intensity, a VPT produces anode signals distributed about a mean value, s, with a variance, σ^2. The relative variance is greater by a factor F, the excess noise factor, than would be expected from a consideration of fluctuations in the number of photoelectrons, n_e, alone. Thus:

$$(\sigma/s)^2 = F/\,n_e \qquad 2$$

F receives contributions from two sources: the reduction, by the grid transmission factor, ε, in the number of photoelectrons contributing to the multiplication process, and fluctuations in the multiplication process itself. Thus:

$$F \approx (1 + 1/M)/\varepsilon \qquad 3$$

where M is the average number of secondary electrons collected at the anode for each photoelectron striking the dynode ($M \sim m(1 - \varepsilon^2)$).

For $m = 20$ and $\varepsilon = 0.6$, equation 3 predicts $F \approx 1.75$. In practice, F varies substantially with the operating conditions in a way that depends on the design of the tube, and values of order 3 are typical.

It is therefore important to take this parameter into consideration when striving to optimise the overall performance.

3 Measured Characteristics

3.1 Response as a function of bias voltage

A vacuum phototriode is a three terminal device. For the CMS application, the electrical configuration chosen has the photocathode at earth potential and positive voltages applied to the dynode and anode. This arrangement minimises the danger of discharges and leakage currents occurring between the tube envelope and the surrounding mechanical structure, but it requires high voltage decoupling between the anode and the preamplifier front end of the electronic readout.

Two considerations are important in establishing suitable values for the bias potentials: the dynode voltage with respect to the photocathode, V_D, should be high enough to obtain a large secondary emission coefficient, and the strength of the field between the dynode and the anode, proportional to $V_A - V_D$, should be sufficient to ensure efficient collection of secondary electrons at the anode. In practice, the anode voltage is set at the highest value that can be sustained without risk of discharges within the tube (or within the external circuitry and cables), and the dynode voltage is chosen which gives the maximum response. As noted below, the optimum dynode voltage at a given anode voltage tends to be somewhat lower in the presence of a magnetic field.

Several different test set-ups were used, designed to allow both dc and pulsed measurements to be made. In a typical arrangement, the VPT viewed a single pulsed light emitting diode (LED) or four dc-excited LEDs from a distance of approximately 60 mm. In this case, the LEDs were 'Hyperbright blue'[15] devices with a peak emission wavelength at 430 nm, well matched to the scintillation emission of lead tungstate. A diffuser, consisting of a single sheet of 80 gsm photocopier paper, was placed midway between the LEDs and the VPT faceplate, to ensure uniform illumination. A diagram of the associated electrical circuit is shown in figure 6. Pulsed signals were taken from the anode, dynode and cathode. In addition, the photocathode and anode currents were measured via the voltage drop across 1 MΩ resistors in series with the cathode and anode leads. Measurements were taken with and without excitation of the LEDs, allowing values of the dark current, photocurrent, and dc gains to be determined as a function of the bias voltages.

Figure 7 illustrates the variation in gain, G, of a VPT, as a function of V_D, for $V_A = 800$ V and $V_A = 1000$ V. The two curves are almost identical up to $V_D = 600$ V, showing an initial rapid rise in G with increasing voltage, followed by a flattening-off as the secondary emission coefficient saturates. For values of V_D above 600 V, the curve for $V_A = 800$ V flattens more rapidly as $V_A - V_D$ falls below 200 V and the collection efficiency at the anode starts to decrease. The curve for $V_A = 1000$ V shows a similar trend above 800 V.

3.2 Response as a function of magnetic field

The uniformity of illumination of the photocathode is a critical consideration when investigating the response as a function of magnetic field. The photocathode covers the whole of the inside of the front window and extends on to the side wall. In the absence of a magnetic field, the full area of the photocathode can contribute to the tube response, since electrons follow the electric field lines and are transported efficiently to the dynode and anode. When a strong magnetic field is applied, the electrons spiral tightly along the magnetic field lines. If the magnetic field is parallel to the axis of the tube, electrons from the perimeter of the photocathode tend to miss the anode and dynode, which necessarily have diameters smaller than the internal diameter of the tube. As a result, the decrease in response with increasing magnetic field is in general smaller if the illumination is concentrated towards the centre of the photocathode, compared to what is observed for uniform illumination. (It

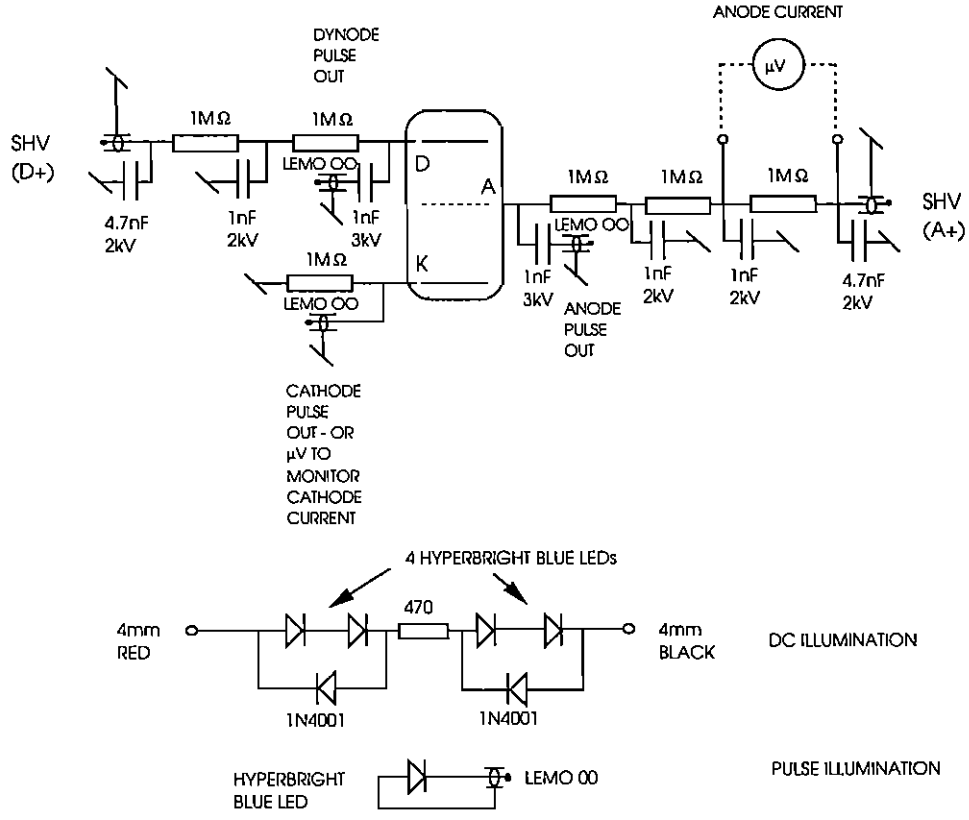

Figure 6: The circuit diagram of a typical test set-up used to measure characteristics of VPTs, with dc and pulse signals.

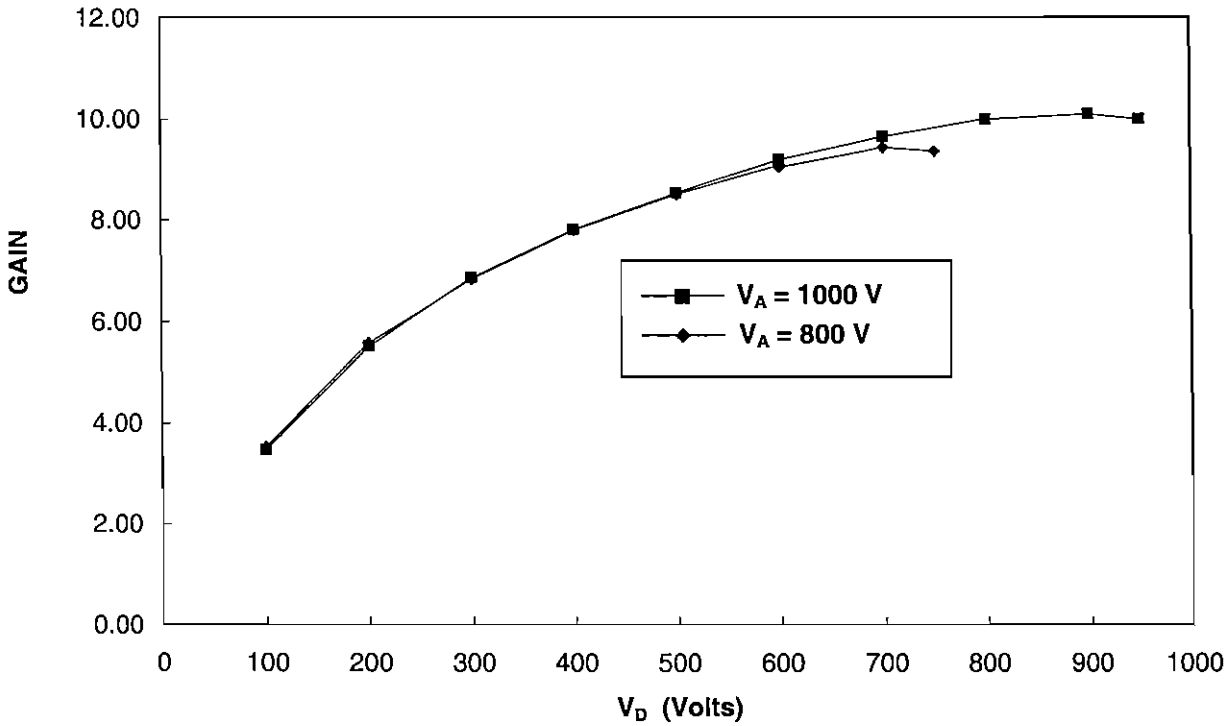

Figure 7: Typical curves of the variation in dc gain versus dynode voltage, V_D, for two values of the anode voltage, V_A. In this case, the VPT has a dynode mesh with 2000 lines per inch (12.7 μm pitch).

should also be noted that the wavelength of light used for the measurements can also affect the results, since bialkali photocathodes may show a much stronger non-uniformity over their area in response to green light, compared to blue.) Since in CMS, the VPT diameter is less than the transverse dimensions of the lead tungstate crystal, measurements made with uniform illumination are more relevant to understanding the performance expected in that application.

If the magnetic field is at an angle to the tube, the region of the photocathode participating in the tube response is displaced and photocathode material deposited on the side wall of the tube may even contribute in this case. Thus the distance between the photocathode and the anode/dynode structure is an important consideration in the design of a tube required to operate in a non-axial magnetic field.

In the presence of a magnetic field, the optimum values of the bias voltages are modified. For a given anode voltage, better performance is obtained with a value of the dynode voltage which is lower than the optimum for zero magnetic field. Even though this results in a lower secondary emission coefficient, the loss is more than compensated by an improved collection at the anode, resulting from the increase in $V_A - V_D$.

Three facilities have been used for investigating the response of VPTs as a function of magnetic field. One (at RAL) enabled measurements to be made at arbitrary field values up to 1.9 T. A second facility (at Brunel) provided a much stronger fixed field of 4.7 T. Finally, access was gained for a short period to a large magnet facility in the North Experimental Area of the SPS at CERN, allowing measurements to be made as a function of magnetic field up to 3.0 T

Figure 8 shows the relative anode response as a function of the magnetic field strength, for a tube with an anode mesh of 2000 lines per inch, measured with the tube axis parallel to the magnetic field, and also with the axis at 15^o to the field. In both cases there are small amplitude excursions in response at low fields, but the main feature is a steady, slow decrease in output with magnetic field up to the highest measured value of 1.8 T. The fall-off with field is significantly less at 15^o compared to 0^o. This behaviour is a common feature of all the tubes tested and is attributed to the way in which the helical electron trajectories pass through the anode mesh. The probability of an electron passing through the mesh depends not only on the radius of the trajectory relative to the mesh size, but also on the pitch of the helix, the thickness of the mesh and the angle between the axis of the helix and the plane of the mesh. The response as a function of angle to the magnetic field is discussed further in the next section.

3.3 Response as a function of magnetic field orientation

In CMS the VPTs are oriented at an angle with respect to the magnetic field that varies from 5.7^o at the inner edge of the end cap ECAL to 25.6^o at the outer circumference. To investigate the behaviour of tubes under conditions relevant to CMS, measurements have been made as a function of angle at fixed magnetic field, and at selected fixed values of magnetic field and angle.

Figure 9 shows the variation in relative anode response over the angular range from -90^o to $+90^o$, in a magnetic field of 1.8 T, for a VPT with an anode mesh of 1000 lpi. There is a significant increase in response as the angle of the tube axis is increased with respect to the magnetic field, reaching maximum values at angles of $\pm 30^o$. (The response curve is not expected to be exactly symmetric about 0^o because the electrode structure is supported at three points 120^o apart in azimuthal angle.) The response remains above the 0^o value at angles up to $\pm 45^o$, before falling sharply. It can be seen from figure 9 that the scope for applying VPT technology to detector design is by no means restricted to applications where the tube axis is aligned with the direction of the magnetic field.

Figure 10 shows the relative anode response as a function of field up to 3 T, for representative examples of three different designs of VPT. One tube has an anode mesh of 2000 lpi, the other two tubes were supplied by a different manufacturer and have meshes of 1500 lpi and 1000 lpi

respectively. The measurements were made with the tubes were aligned at an angle of 15^{o} with respect to the field, corresponding to a region at approximately the centre of the acceptance of the CMS ECAL end caps. The general expectation is that the finer the anode mesh, the smaller will be the relative loss in response at high magnetic field. It is interesting to note that for these designs, with the field aligned at 15^{o} with respect to the tube axis, the tubes with the coarser meshes show smaller losses in response for fields up to 3 T, although the output of the 1000 lpi tube is falling above 1.5 T.

4 Accelerated ageing tests

4.1 Prolonged operation with high photocathode currents

At the LHC, the high luminosity and the high collision energy will lead to very intense fluxes of secondary particles within the CMS detector. Thus although lead tungstate has a relatively low scintillation yield, the time averaged light output from the crystals in the ECAL end caps will be high, producing substantial photocurrents in the VPTs during operation. An estimate based on the expected radiation levels in the ECAL (figures 3a, 3b), with the LHC running at full luminosity, predicts a value of the mean photocurrent of 0.1 nA at outer radius of the end cap, increasing to 2.5 nA at $|\eta| = 2.5$, and 8 nA at the inner circumference. It is essential that the VPTs can be operated at such currents for at least ten years of LHC running, without suffering significant degradation.

In order to investigate possible ageing effects, tubes have been operated with a high photocathode current for an extended period, both in the absence of a magnetic field and in an axial field of 1.8 T. A standing current was induced in the tube by illuminating the photocathode with an LED, excited by a constant current. The response of the tube was measured concurrently with the dc illumination by measuring the anode signal induced by pulsing a second LED of the same type. Both LEDs were arranged to give uniform illumination of the photocathode.

Tests on most tubes were conducted with the excitation current in the dc LED adjusted to produce an initial value of the photocurrent, I_k, of 100 or 200 nA, although measurements were also made with $I_k = 10$ nA and $I_k = 1$ μA. Bialkali photocathodes can have very high surface resistivities (of order $R_{\square} = 10^{10}\ \Omega$), which might lead to substantial potential gradients across the photocathode at large values of I_k, modifying the operation of the tube. However, no evidence was seen for any substantial effect of this nature. For example, the instantaneous effect on the anode response to the pulsed diode, caused by switching the dc diode on/off, was small. Furthermore, detailed measurements on one of the tubes showed that the gain was constant over a very wide range of photocurrents.

Figure 11a shows the relative anode response as a function of time for a tube operated with a photocurrent of 1 μA. The first sequence of measurements was made in an axial magnetic field of 1.8 T. The response shows a rapid decrease over a period of a few hours to 80% of the initial value, then falls more slowly to plateau at 75% after 6 days. (In terms of integrated charge drawn from the photocathode, 6 days of ageing at $I_k = 1$ μA corresponds to approximately 18 years of LHC running for a VPT at $|\eta| = 2.5$ in the CMS ECAL end cap.) The magnetic field was then set to zero and the ageing continued. Renewed degradation in anode response was observed, resulting in a fall to 60% of the initial value (corrected for the effect of magnetic field on gain) after two days. Finally, the magnetic field was returned to 1.8 T and ageing continued for a further day. During this period, the relative anode response was found to remain stable at approximately 60%.

The general features displayed in figure 11a have been observed in tests on a number of tubes of different designs, although the time constants and magnitudes of the effects vary. Figure 11b shows a sequence of measurements made on a tube from a different manufacturer. In this case the initial value of the photocurrent was 200 nA. Again there is a rapid decrease in response during the first few hours of operation at 1.8 T, with an eventual plateau at 80% reached after several days. (There is a hint that

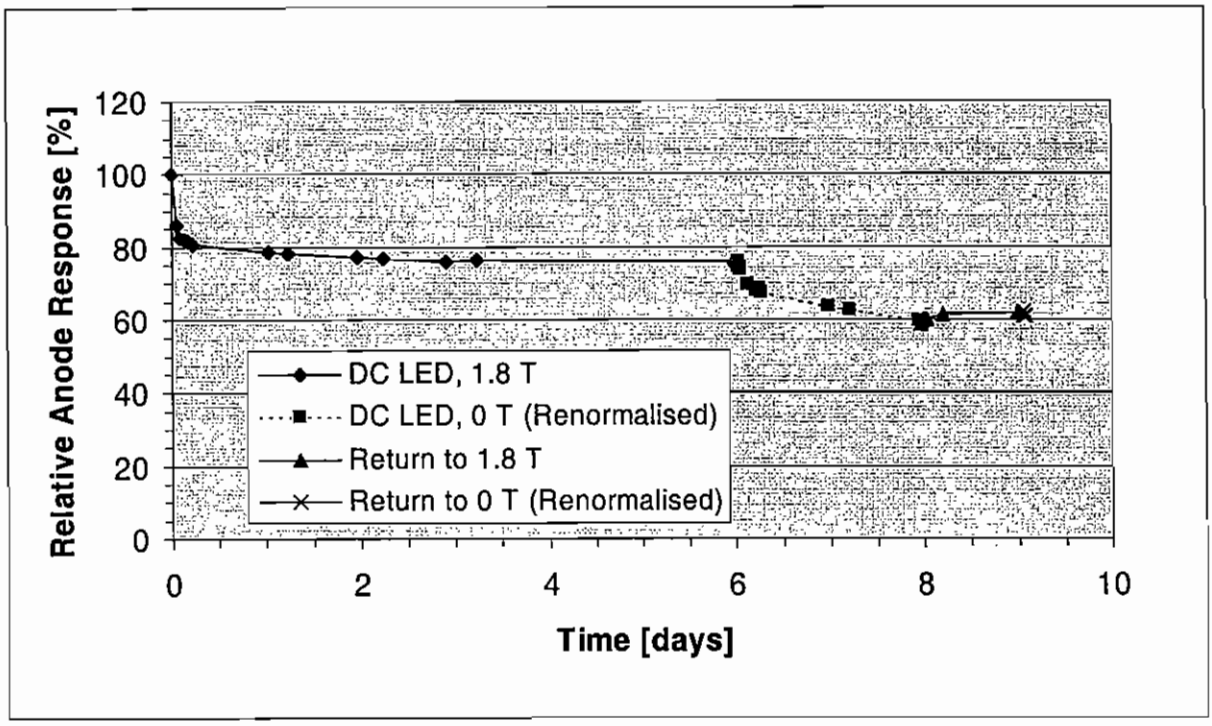

Figure 11a: Relative anode response as a function of time with a standing photocathode current, $I_k = 1$ μA. The VPT has an anode grid with 400 lpi (63.5 μm pitch).

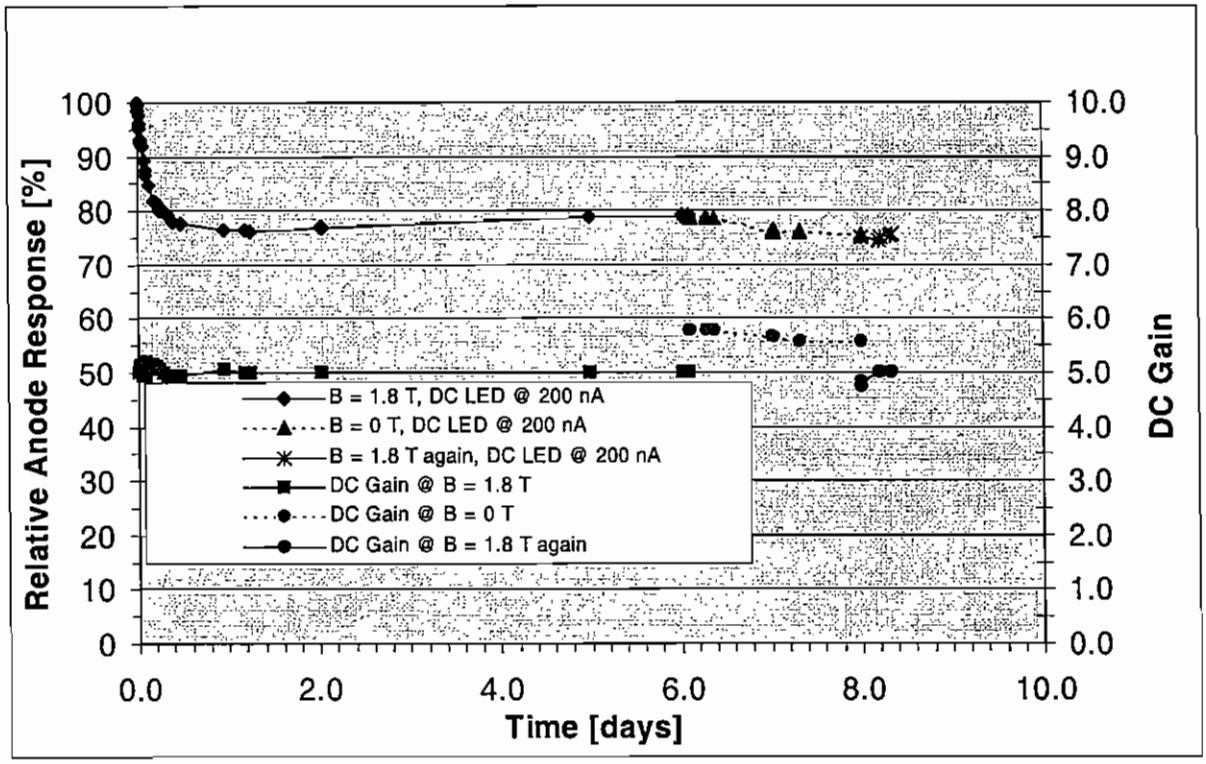

Figure 11b: Relative anode response (left hand scale) and dc gain (right hand scale) as a function of time with a standing current, $I_k = 200$ nA. The VPT has an anode grid with 2000 lpi (12.7 μm pitch).

the initial fall is somewhat larger and that it is followed by a slight recovery.) After six days the field was reduced to zero for two days, and again a further loss in response was observed which remained after the field was returned to 1.8 T.

Also plotted in figure 11b is the ratio of the anode and cathode currents as a function of time. In the absence of a significant anode-to-dynode dark current, the anode/cathode current ratio is equal to the gain. The ratio remains constant over the first six days at a magnetic field of 1.8 T. It rises discontinuously when the field is set to zero, (as expected from the normal effect of magnetic field on gain), then shows a small decrease. The decrease is probably associated with a change in dark current rather than a change in gain, since when the field is returned to 1.8 T, the anode/cathode current ratio rapidly returns to the previous value at this field, after starting slightly lower. The constancy of the anode/cathode current ratio over the first six days of the study, and the return to the initial value at the end, shows that overall fall in anode response of the tube is associated with a loss in photocathode efficiency, rather than a decrease in gain.

The measurements presented in figure 11a, made with $I_k = 1$ μA, have been repeated at $I_k = 10$ nA and $I_k = 100$ nA respectively, on two other tubes of identical design. The results are compared in figure 12. It can be seen that the initial fall in response occurs most rapidly for $I_k = 1$ μA, slightly more slowly for $I_k = 100$ nA, and significantly more slowly for $I_k = 10$ nA. However, after 24 hours, the anode response has plateaued at approximately 80% of the initial value in all three cases.

The observed features; namely, an overall loss in photocathode response (but not gain) which is initially rapid and dependent on the tube current, but which finally reaches a current independent plateau, may be explained in terms of the effect of residual gas in the tube. A large photocurrent will ionise the gas, releasing positive ions that will be collected on to the photocathode, degrading the efficiency for photo-emission. If this hypothesis is correct, then decreasing the residual gas pressure in the tube, by incorporating a getter, should substantially decrease the ageing. Figure 13 shows the results obtained with a gettered tube of similar design to that of figure 11b. In marked contrast to figure 11b, the relative anode response remains extremely constant throughout 25 days of operation at $I_k = 200$ nA. This gives strong support to the postulate that the ageing behaviour under strong illumination depends primarily on the quality of the tube vacuum.

4.2 Irradiation studies

Over the lifetime of the CMS experiment, the VPTs in the ECAL end caps will be exposed to very large integrated doses of radiation in the form of charged particles, γ-rays and neutrons. The estimated doses and particle fluences for 10 years of LHC operation are shown in Figures 3a and 3b. Typical values for the dose are 0.5 kGy at the outer circumference of the end cap ($|\eta| = 1.5$), 3.0 kGy at $|\eta| = 2.0$, 20.0 kGy at $|\eta| = 2.6$, and 50.0 kGy at the inner edge ($|\eta| = 3.0$). Representative values of the neutron fluence are 5×10^{13} n/cm^2 at $|\eta| = 1.5$ and 7×10^{14} n/cm^2 at $|\eta| = 2.6$.

In general, the most important effect of ionising radiation on vacuum photodetectors is a darkening of the glass envelope. Borosilicate glass, which is normally used for phototube windows, is particularly susceptible to such damage (figure 14) and, even at quite low radiation doses, the loss in transparency substantially reduces the effective photocathode efficiency. Fused silica ('quartz') is much more radiation resistant than borosilicate glass and is frequently used for the faceplates of phototubes required to operate in high radiation environments. However, the thermal properties of fused silica differ markedly from the properties of glasses normally used to fabricate the rest of the phototube envelope. Incorporating a fused silica window therefore requires the use of graded seals, complicating the manufacturing process and adding substantially to the cost. In the course of developing VPTs for CMS, effort was therefore devoted to identifying cost effective alternatives to fused silica, with adequate radiation resistance. The initial objective was to find a material which can be used for tubes in the region $1.5 < |\eta| < 2.6$, covering approximately 95% of the end cap detectors,

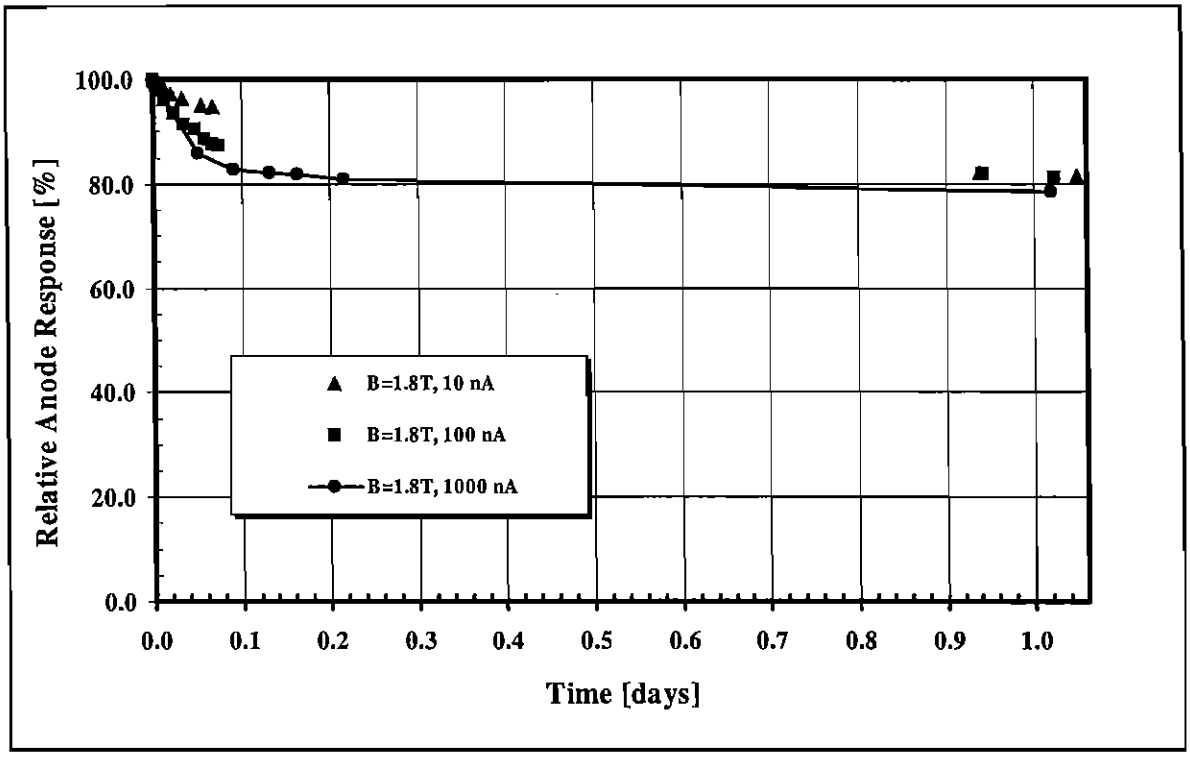

Figure 12: Relative anode response as a function of time for three tubes of identical design, under different levels of illumination producing $I_k = 10$ nA, $I_k = 100$nA, and $I_k = 1\mu$A, respectively. The $I_k = 1\mu$A values are a subset of those plotted in Figure 11a.

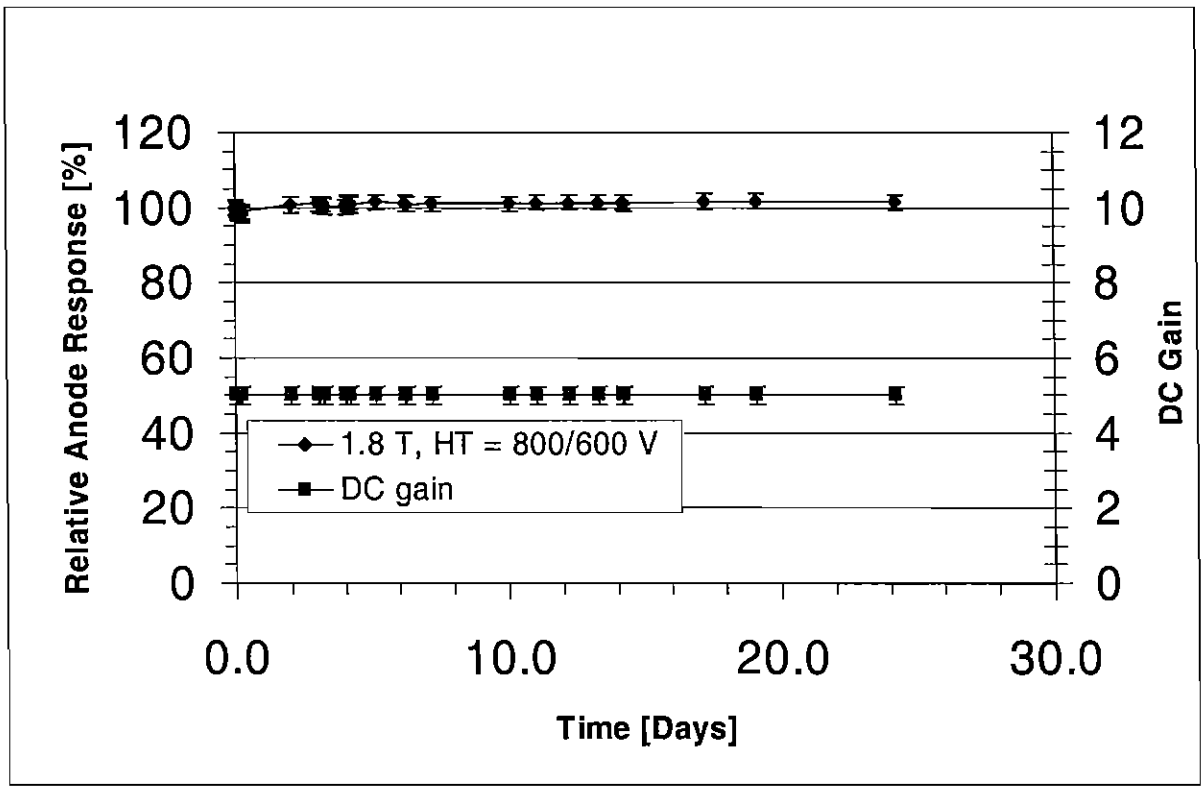

Figure 13: Relative anode response as a function of time with a standing photocathode current, $I_k = 200$ nA. This VPT has a getter, but is otherwise identical to that of Figure 11b.

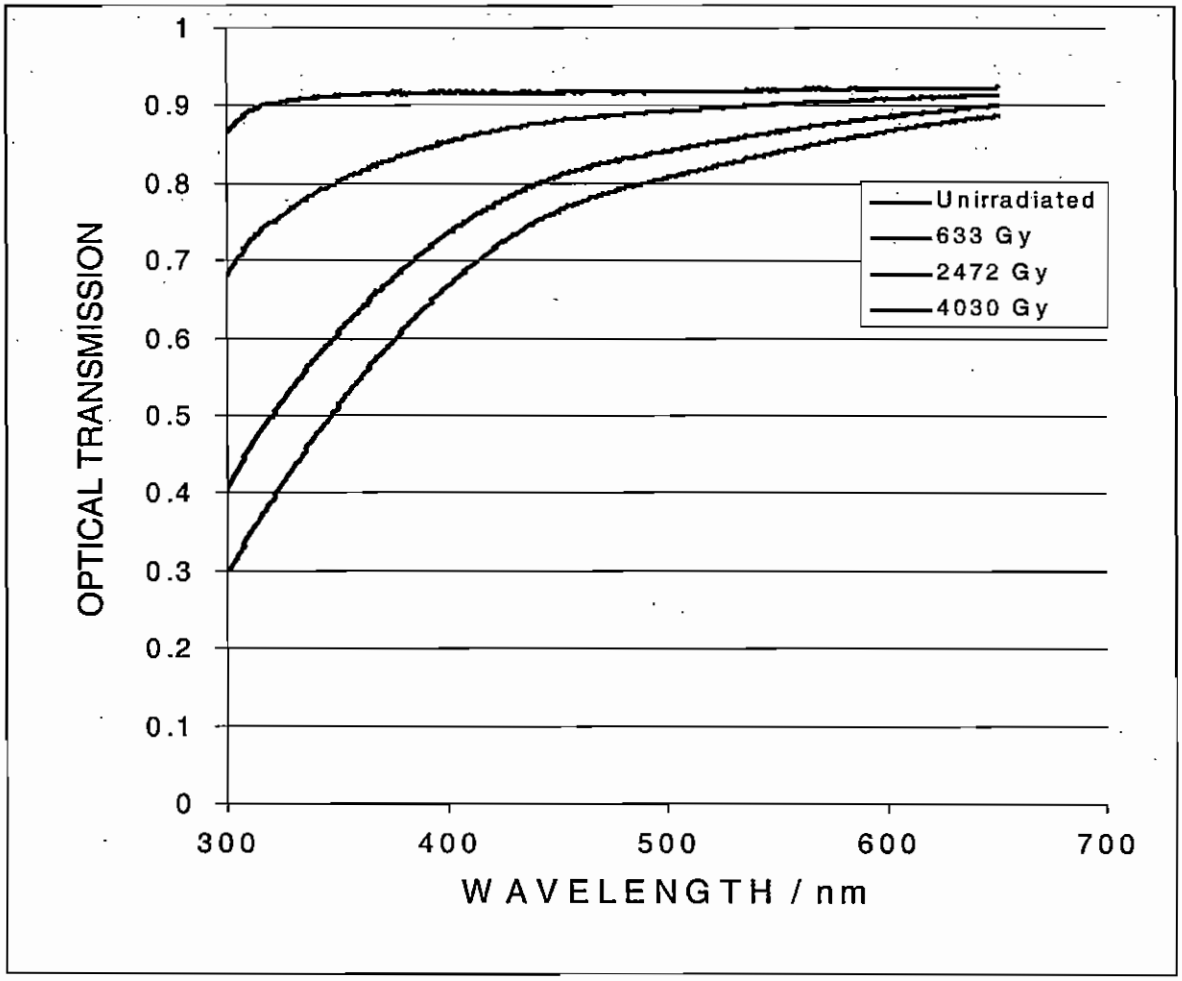

Figure 14: The external optical transmission as a function of wavelength for a 1 mm thick sample of borosilicate glass, before and after successive exposures to γ radiation from a ^{60}Co source. The transmission before irradiation is less than unity because of losses by Fresnel reflection at the glass surfaces.

and to leave open the possibility of using fused silica tubes for the innermost part, where the radiation levels are substantially higher.

Radiation resistant glasses containing cerium are readily available commercially. Such glasses are able to withstand very high radiation doses without suffering significant darkening. However, the unirradiated absorption band edge typically occurs in the blue region and cuts into the emission spectrum of lead tungstate. Furthermore, the thermal properties are not ideal for phototube applications and give rise to problems similar to those encountered with fused silica.

In addition to its susceptibility to radiation damage, another shortcoming of borosilicate glass is its poor transmission in the near ultraviolet. Special glasses with enhanced UV transmission have therefore been formulated for use in phototubes. Although not specifically developed to be radiation hard, a consequence of the improved UV transmission is that the radiation induced colour centres also occur at shorter wavelengths, and darkening at wavelengths above 400 nm is strongly reduced. To investigate if such glasses are sufficiently radiation hard for application in CMS, irradiation studies were made using a ^{60}Co radioactive source. The results presented below are for faceplate samples kindly provided by Electron Tubes Ltd[5] and Hamamatsu[6].

The irradiations were performed in 10 kGy steps, in the dark at a constant temperature of 19.5° C. The dose rate was 432 Gy/hr, thus a 10 kGy exposure took approximately 24 hours. The dose in air was measured and corrected to a dose in Pyrex glass (80% SiO_2). Optical transmission measurements were made within one hour of the end of each irradiation.

Figure 15a shows the external optical transmission as a function of wavelength for a 1.0 mm thick faceplate sample, at the start and after successive irradiations up to 30 kGy. The first two exposures were made in quick succession; the final exposure to reach 30 kGy was made 24 days after the second. The measured transmission before irradiation is less than unity because of losses by Fresnel reflection at the surfaces of the sample. The exposures were made at dose rates many times greater than those which will be encountered during the operation of CMS, even at the inner edge of the end cap calorimeter ($|\eta| = 3$). Such an accelerated test can give a pessimistic prediction of the expected damage since self-annealing of colour centres will reduce the asymptotic loss of transparency for a given dose delivered over a longer period. Figure 15a also shows the transmission measured after the sample had been stored in the dark for 24 days at room temperature following the second exposure. It can be seen that significant self-annealing occurred.

A comparison of figure 15a with figure 14 shows that this UV glass is much more radiation resistant than borosilicate glass but still shows significant radiation darkening, especially at short wavelengths. For the CMS application, the parameter of interest is the loss in transmission of scintillation light from lead tungstate, to be expected after a given radiation exposure. This is estimated by folding the irradiated transmission spectrum with the scintillation emission spectrum of lead tungstate, shown in figure 4. The resultant integrated transmission is shown as a function of dose in figure 15b.

The design objective is to ensure that the loss in response of the VPTs to scintillation light from lead tungstate is less than 10% after 10 years of operation. It can be seen that the glass of Figure 15b satisfies this criterion with a substantial margin of safety for doses below 20 kGy, especially when the effect of self-annealing is allowed for. Only the inner part of the end cap, covering the pseudorapidity range $2.6 < |\eta| < 3.0$ (5% of the total area), is expected to receive doses greater than this.

4.3 Helium ingress

Ageing caused by prolonged operation at high photocurrents and darkening of the faceplate by radiation are two possible sources of damage in VPTs. A third effect, with possible implications for operation in CMS, is ingress of helium. It is well known that, over a period of time, helium can diffuse through the envelope of a phototube and degrade the performance. The helium is ionised by

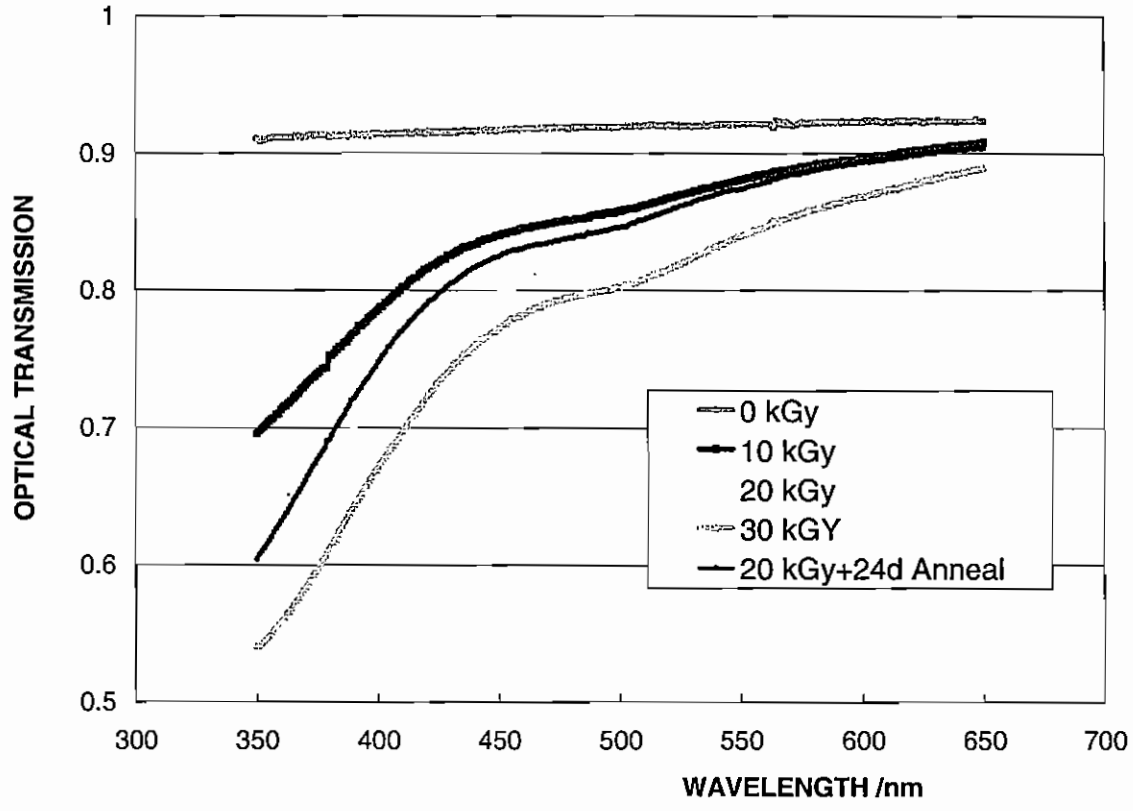

Figure 15a: The external optical transmission as a function of wavelength for a 1.0 mm sample of UV-transmitting glass, before and after successive exposures to γ radiation from a ^{60}Co source. The glass was allowed to anneal for 24 days in the dark before the final exposure. (The transmission before irradiation is less than unity because of losses by Fresnel reflection at the glass surfaces.)

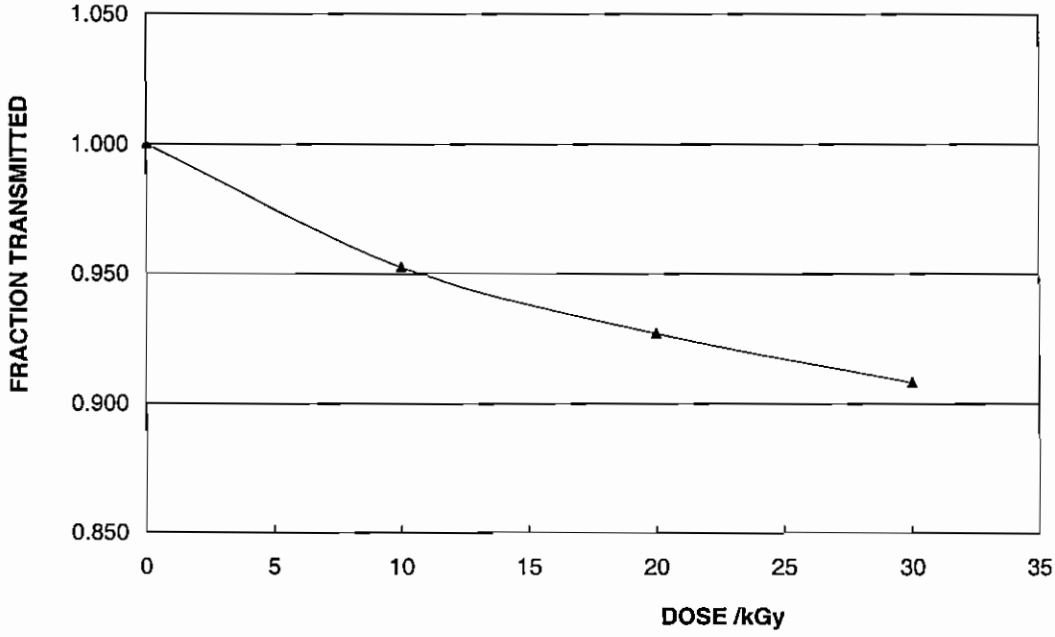

Figure 15b: The estimated loss in transmission of scintillation light from $PbWO_4(La)$, through the glass sample of Figure 15a, following ^{60}Co irradiation.

the photocurrent, producing positive ions that are accelerated towards the photocathode, where they impact to produce additional electrons. As the helium pressure rises, electron multiplication can start to occur in the helium, dramatically increasing the anode signal. Eventually, at pressures of order 1 Pa, electrical breakdown occurs. The risk is greatest for tubes with a fused silica window and/or envelope, but it cannot be neglected for devices constructed with borosilicate glass. The natural partial pressure of helium in the atmosphere is 0.7 Pa and exposure of a phototube to helium at this concentration can result in an average life of 10 years[16].

The LHC uses superconducting magnets and has an enormous associated cryogenic system. Furthermore the CMS detector itself incorporates a very large superconducting magnet. It is therefore prudent to assume that the helium concentration in the vicinity of the CMS experiment will be somewhat above the normal ambient level, and could rise very much higher in the event of a failure in the cryogenic system. To protect the VPTs from possible damage from this source, the detector volume surrounding them will be flushed with nitrogen. Nevertheless, as part of the development programme, studies were made to understand better the susceptibility of VPTs to the external presence of helium.

The pressure, $P_I(t)$, within a tube after a time, t, immersed in an atmosphere with helium at partial pressure, P_E is given by the expression:

$$P_I(t) = P_E\,(1 - e^{-ct}) \qquad 4$$

with

$$c = 10^5\,D\,A\,(T/273)/d \qquad 5$$

where A is the aspect ratio of the VPT, defined as the ratio of the surface area of the envelope to the enclosed volume ($A \approx 2$ cm^{-1} for 25 mm diameter VPTs), T is the absolute temperature, and d is the thickness of the glass envelope (of order 1 mm). D is the helium diffusion coefficient and is temperature dependent. For borosilicate glass at 20°C it has the value[17]:

$$D = 5.7\times10^{-16}\,(\text{cm}^3 \text{ at NTP})/\text{s}/\text{cm}^2/(\text{Pa/mm thickness})$$

Thus equation 4 predicts that after 10 years exposure to an atmosphere containing helium at the normal ambient pressure of 0.7 Pa, the pressure inside a 25 mm VPT would have risen to 2.6×10^{-2} Pa.

In order to gain a better understanding of the likely mode of failure of a VPT subjected to prolonged exposure to helium, an empirical investigation was made. For this test, a tube with a UV-transmitting glass window was enclosed in a gas-tight box, and excited with a pulsed LED light source set to produce anode signals of 50 ns width and 100 μA amplitude at a repetition rate of 1.4 kHz. Bias voltages of -800 V and -200 V were applied to the cathode and dynode respectively, with the anode at earth potential. Both the anode signal pulse and the mean anode current were monitored for the duration of the test.

Initially the tube was operated for several days under dry nitrogen to allow the system to stabilise. The gas supply was then changed to pure helium. However, it was discovered that electrical breakdown rapidly occurred within the enclosure (external to the tube) under this condition. The test was therefore continued with a mixture of 70% helium and 30% nitrogen. The measured anode current as a function of time is shown in figure 16. No discernible effect was visible for approximately the first 5 days of helium operation. After that, the current started to increase, rising by 10% of the initial value during the next 5 days. This increase in the mean current was clearly associated with the appearance of a tail, with a time constant of several tens of nanoseconds, on the trailing edge of the pulse signal. In the following 20 days the current in the tube rose dramatically, reaching ten times the starting value before internal breakdown finally occurred after 50 days. By that time, the anode pulses induced by the LED were of order 1μs long. Equations 4 and 5 predict that helium pressure in the tube would have reached approximately 20 Pa when breakdown occurred.

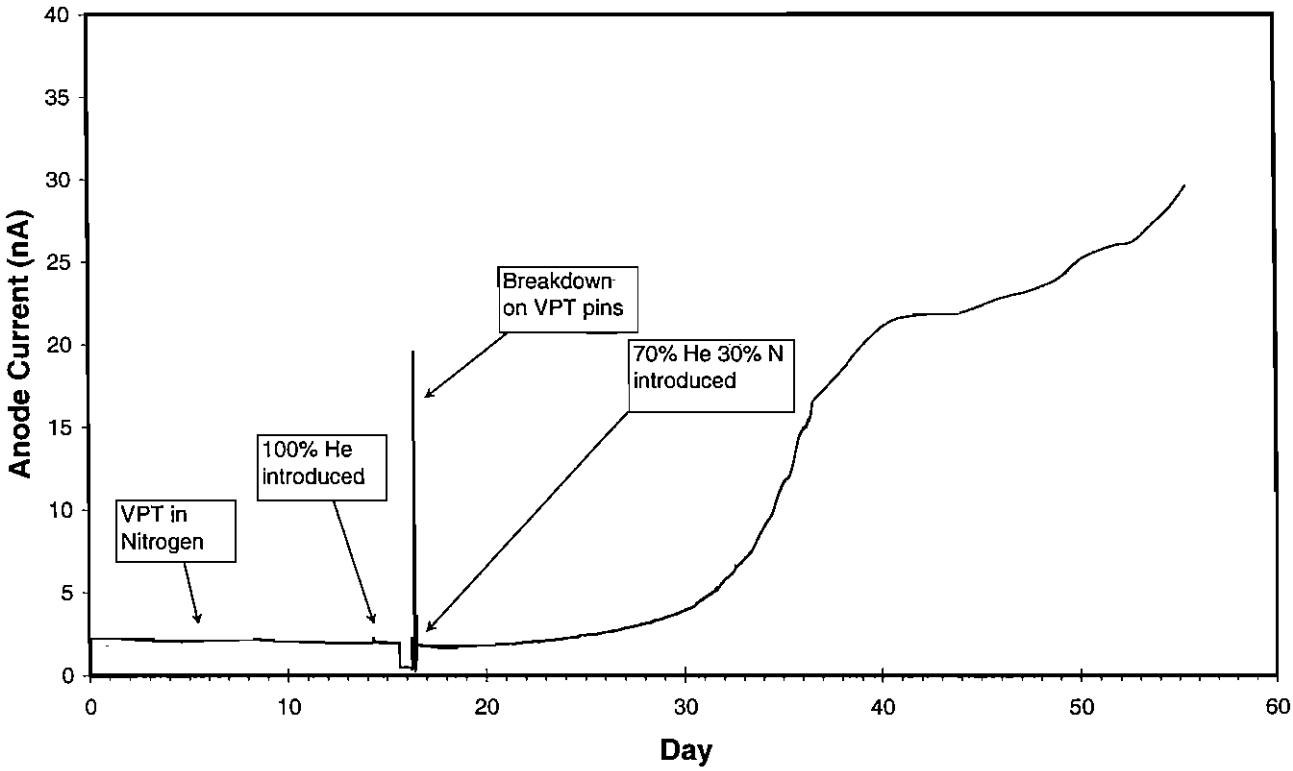

Figure 16: The evolution of anode current with time for a VPT illuminated with a pulsed light source and operated in a helium-rich environment.

Although there was a significant delay before serious degradation occurred, with a helium concentration that was 10^5 times greater than the normal concentration in the atmosphere, the results must be interpreted with caution, since it will have taken several days for the helium to diffuse through the glass envelope and start to contaminate the vacuum. Nevertheless, it is reassuring to note that even after the first onset of a detectable effect, an additional five days elapsed before a 10% tail had been added to the signal pulse. Furthermore, the deterioration was progressive and was not characterised by early catastrophic discharges.

In view of the relative graceful failure of the VPT in the above test, and the precautions that will be taken to avoid exposure of the VPTs to helium in CMS, it is concluded that helium ingress does not pose a significant threat for this application.

5 Test of a prototype ECAL module in a high energy electron beam

The final step in the development of vacuum phototriodes for CMS was a demonstration that a prototype ECAL module, instrumented with these devices, could achieve the designed energy resolution. To this end, a basic sub-unit of the ECAL end cap detector was constructed. This consisted of a 5x5 array of crystals of the correct dimensions, supported by a thin wall, carbon fibre 'alveola' structure, contained in a temperature stabilised enclosure. The crystals were instrumented with a mixture of different types of VPT, supplied by three manufacturers[5,6,8]. Measurements were made at six energies in the range from 15 GeV to 180 GeV, in a high energy electron beam (H4) at CERN[18].

In CMS, a 'pre-shower' detector is located immediately in front of the end cap crystal arrays, to provide a precise measurement of the impact points of high energy photons entering the calorimeter. This consists of a lead converter, 2 radiation lengths thick, followed by a plane of silicon strip detectors, followed by 1 radiation length of lead, followed by a second plane of silicon strips. To provide a fully realistic simulation of the CMS configuration, a prototype pre-shower detector was therefore incorporated in the test beam set-up for some of the measurements.

The first set of measurements was made with the crystal array alone. A set of calibration constants was established by moving the array to centre each crystal in turn on the beam, and recording 40 000 events at an energy of 50 GeV. The beam was then directed into each of the central nine crystals of the 5x5 array, and 100 000 events recorded at each of six energies. For each event, the energy deposited in the array was taken as the sum of the energy recorded in the crystal on the beam axis together with the energies in the eight crystals immediately surrounding it. After correction for electronic noise, the energy dependence of the energy resolution was found to be well described by an expression of the form:

$$\sigma_E/E = A/\sqrt{E} \oplus C \qquad 6$$

where A is the 'stochastic' coefficient, determined by photoelectron statistics and the excess noise factor of the VPT. The constant term, C, receives contributions from non-uniformity of the crystal response as a function of depth, shower leakage from the rear of the crystals, inter-channel calibration errors and energy absorption in inert material. The constant term dominates the resolution function at high energy.

Typical values for A and C, obtained with the beam directed into the central crystal of the 5x5 array, were: $A = (4.2 \pm 0.4)\%$, $C = (0.23 \pm 0.05)\%$, with E expressed in GeV.

A second set of measurements was made with the pre-shower detector place in front of the crystal array. As expected, the energy resolution was degraded by the lead converters of the pre-shower detector. However, the loss in resolution was recovered to a large extent by correcting for energy loss in the lead, using pulse height information from the silicon strip detectors. Figure 17 shows the

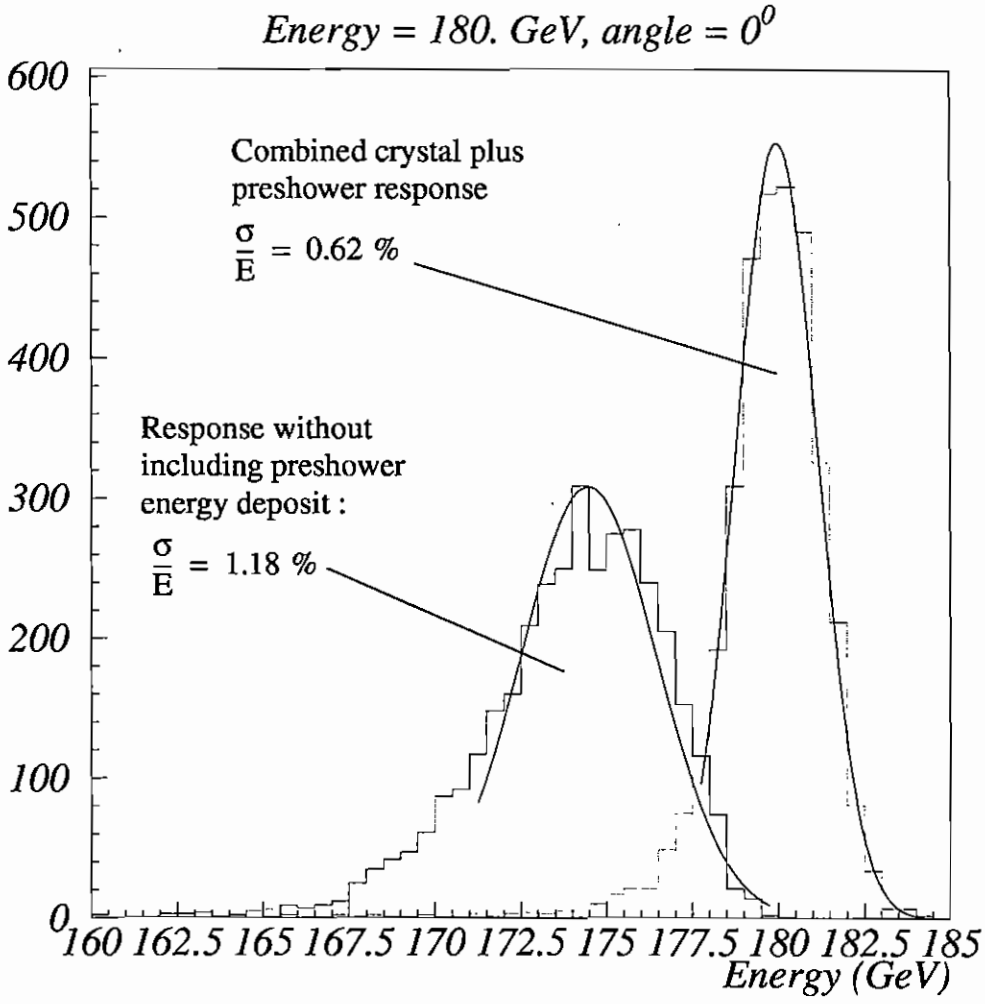

Figure 17: The Energy distributions measured in the prototype crystal array, before and after correction for energy loss in the pre-shower detector.

energy distribution at 180 GeV, with and without this correction. The corrected energy resolution is 0.62%, which fully meets the performance requirements for CMS at this energy.

At low energies, electronic noise contributes substantially to the resolution function; it was therefore important to establish that the required noise performance could be achieved. The energy equivalence of the noise depends on the electronic noise in the readout chain (particularly the preamplifier); the gain, quantum efficiency and effective photocathode area of the VPT and the light yield of the crystal. The final form of the CMS readout electronics was not available for the beam tests; it was therefore necessary to estimate the expected noise performance from the measured characteristics of the crystal/VPT combination and the design parameters of the final electronic system. Since the beam measurements were made without a magnetic field, it was also necessary to correct for the loss in VPT gain expected at the CMS operational field of 4 T.

There was a considerable spread in the measured performance of different designs of VPT, and in the light yields of the crystals. Furthermore, there was some uncertainty in extrapolating to the performance of the final electronic system. Nevertheless, the measurements showed that several designs of VPT should be capable of meeting the CMS design goal of 150 MeV/channel equivalent noise energy, with a substantial safety margin.

The light yield of each lead tungstate crystal was measured with a radioactive source and a calibrated photomultiplier tube, prior to installation in the array. It is therefore possible to combine this information with laboratory measurements of the VPT parameters, to estimate the expected relative performance of each VPT/crystal combination in the test beam[19]. Figure 18 shows the distribution of the ratio between the mean anode signal from each channel, estimated from the laboratory measurements, to the signal measured with 50 GeV electrons. The rms width of the distribution is less than 10%, confirming that performance parameters of the VPTs (and the crystals) are well understood.

6 Summary

Vacuum phototriodes have been successfully developed for instrumenting the end cap sub-system of the CMS electromagnetic calorimeter. An extensive programme of tests has demonstrated that the new devices are superior to those previously available in a number of respects, most notably: gain in very high magnetic fields, radiation resistance and stability at large photocurrents.

A model has been developed which allows the operational characteristics to be understood in term of a small number of device parameters.

Measurements on a prototype sub-module of the CMS ECAL, in a high energy electron beam, show that the design goals of the full system can be achieved using this new generation of VPTs.

Other applications requiring high speed, high sensitivity photodetection in very strong magnetic fields could benefit from the use of these devices.

7 Acknowledgements

The authors gratefully acknowledge many useful discussions with their colleagues on the CMS Electromagnetic Calorimeter project, especially with Dr D Seliverstov of Petersburg Nuclear Physics Institute. They extend their thanks to Electron Tubes Ltd, Hamamatsu Photonics and Photonis for their extensive co-operation in this work, to Dr J E Bateman of RAL for the insights provided in VPT operation through his modelling studies, and to Dr R Stephenson of RAL for his help in supplying the low noise bias and amplification circuits essential to many of the measurements.

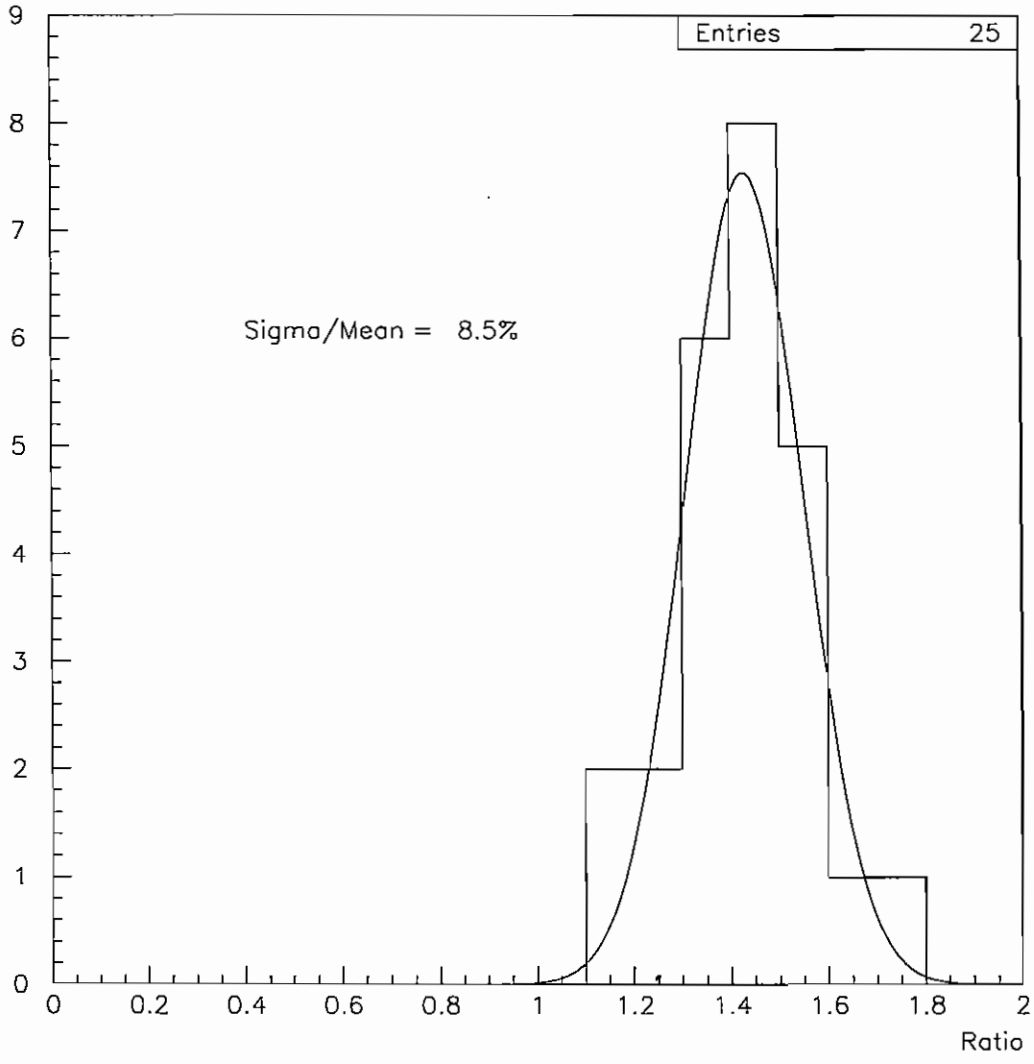

Figure 18: The distribution of ratios of (predicted signal)/(measured signal) for the 25 channels of the ECAL prototype array. The predicted signal is the product of laboratory measurements of the crystal light yield and the photocathode sensitivity and gain of the VPT. The measured signal is the mean of the anode charge distribution recorded with a 50 GeV electron beam directed into the centre of the crystal. The quantity of interest is the width of the distribution (the absolute normalisation is arbitrary).

References

1 The Compact Muon Solenoid Technical Proposal,
CERN/LHCC 94-38, 1994.

2 The CMS Electromagnetic Calorimeter Project Technical Design Report,
CERN/LHCC 97-33, 1997.

3 *Properties of the avalanche photodiodes for the CMS electromagnetic calorimeter*,
K Deiters et al., Nucl Instr and Meth, A453 (2000), 223-226.

4 *Fast neutron irradiation of some APDs proposed for application in the CMS ECAL*,
J E Bateman et al., RAL Technical Report, RAL-TR-1997-075.

5 Electron Tubes Limited, Bury Street, Ruislip, Middx, HA4 7TA.

6 Hamamatsu Photonics UK Ltd, Lough Point 2, Gladbeck Way,Windmill Hill, Enfield, Middx, EN2 7JA.

7 Photonis, Avenue Roger Roncier, B.P. 520, 19106 Brive La Gaillarde Cedex, France.

8 National Research Institute Electron, Morisa Toreza Ave., 68, 194223 St. Petersburg, Russia.

9 Moscow Electrolamp Factory (MELZ),
105023, Moscow, Electrozarodskaya St. 23, Russia.

10 *Fine-Mesh Photodetectors for CMS Endcap Electromagnetic Calorimeter*,
N A Bayanov et al, Nucl Instr and Meth, A442 (2000), 146-149.

VPTs with anomolous gain,
V V Brekhovxkikh et al., CMS Internal Note, CMS IN-2000/008-ECAL

11 *Development Studies for the OPAL End Cap Electromagnetic Calorimeter Using Vacuum Photo Triode Instrumented Leadglass*,
M Akrawy et al., Nucl Instr and Meth, A290 (1990), 76-94.

12 P Abreu et al., The DELPHI Collaboration, Nucl Instr and Meth, A378 (1996), 57-100.

13 *Performance of some Prototype Phototriodes in Axial and Quasi-axial Magnetic Field up to 4.7T*,
D C Imrie, Brunel University Uxbridge UK, and RAL, Chilton Didcot, UK, Internal Note (1998).

14 *The operation of Vacuum Phototriodes in an Axial Magnetic Field - a Monte Carlo Study*,
J E Bateman, CMS Note 1998/059 (1998) and RAL Technical Report, RAL-TR-1998-059.

The operation of Vacuum Phototriodes in a Non-Axial Magnetic Field - a Monte Carlo Study,
J E Bateman, CMS Note 1999/032 (1999) and RAL Technical Report, RAL-TR-1998-089.

15 'Hyperbright blue' light emitting diode (manufactured by Siemens)
Stock No 284-1392, R.S. Components Ltd., P.O. Box 99, Corby, Northants, NN17 9RS.

16 *Photomultiplier Tubes - Principles & Applications*,
Photonis, BP 520, F-19106 Brive, France.

17 *Glass Science*, R H Doremus, John Wiley & Sons Inc, 2nd edn (1994), p.141.

18 *CMS ECAL End-cap Test Beam Results 1999*,
CMS Note, in preparation.

Results from the 1999 Beam Test of a Preshower Prototype,
P Aspell et al., CMS Note 2000-001.

19 *The performance of prototype Vacuum Phototriodes in the first full sized Supercrystal array for the ECAL End caps*,
B Camanzi et al., CMS Note 2000/054.